Scaling in Nonstationary Voltammetry Representations

Costas A. Anastassiou,*,† Kim H. Parker, and Danny O'Hare

Department of Bioengineering, Imperial College London, SW7 2AZ London, U.K.

Received: June 13, 2007; In Final Form: August 9, 2007

Despite the widespread use of voltammetry for a range of chemical, biological, environmental, and industrial applications, there is still a lack of understanding regarding the functionality between the applied voltage and the resulting patterns in the current response. This is due to the highly nonlinear relation between the applied voltage and the nonstationary current response, which casts a direct association nonintuitive. In this Article, we focus on large-amplitude/high-frequency ac voltammetry, a technique that has shown to offer increased voltammetric detail compared to alternative methods, to study heterogeneous electrochemical reaction-diffusion cases using a nonstationary time-series analysis, the Hilbert transform, and symmetry considerations. We show that application of this signal processing technique minimizes the significant capacitance contribution associated with rapid voltammetric measurements. From a series of numerical simulations conducted for different voltage excitation parameters as well as kinetic, thermodynamic, and mass transport parameters, a number of scaling laws arise that are related to the underlying parameters/dynamics of the process. Under certain conditions, these observations allow the determination of all underlying parameters very rapidly, experiment duration typically ≤ 1 s, using standard electrode geometries and without any *a priori* assumptions regarding their value. The theoretical results derived from this analysis are compared to experiments with an outer-sphere electron-transfer species, $Ru(NH_3)_6^{2+/3+}$, on different electrode materials, and the determined parameters are in excellent agreement with published values.

1. Introduction

Electrochemical sensing methodologies offer excellent spatial and temporal resolution as well as superior microfabrication possibilities and have attracted considerable attention, especially since the advent of miniaturization, to study and monitor a range of chemical, biological and environmental processes.[1,2] More specifically, voltammetry, where the electrode voltage is perturbed according to a predetermined manner, has been shown to offer increased sensitivity and selectivity over alternative electrochemical techniques.[3] As a result, voltammetric methodologies are frequently employed for investigations ranging from the physics of electron transfer (ET)[4] to monitoring the evolution of reactions[5] and multicomponent systems.[6,7]

The most popular voltammetric technique has been cyclic voltammetry (CV) where the voltage excitation imposed on the electrode is a series of cyclic ramps. To study the underlying electrochemical processes, the shape/symmetry of the voltage (input)−current (output) relationship is recorded and translated in terms of theoretical models.[8] In electrochemical reaction-diffusion processes, a situation very commonly encountered in electrochemical dynamics, determination of the species- and process-specific parameters has commonly relied on CV in combination with a number of assumptions regarding the nature of the ET or the fluid flow characteristics (for instance, see the work by Nicholson[8] and Nicholson and Shain[9]).

Another approach for quantification of these parameters has been the combination of CV with specialized electrode geometries and methods to ensure rapid mass transport, normally by the presence of convection, such as impinged jets.[10−15] Under such conditions, the characteristics of the voltammogram are attributed to kinetic limitations because these are assumed to be the rate-determining step of the overall process. The same principles are used in nanopore electrodes and scanning electrochemical microscopy, where the very small size of the electrode and fast diffusion rates allow the investigation of fast electrochemical kinetics as well as coupled chemical reactions.[16−20] Although accurate, such methods require specialized devices that are expensive and rather restrictive in application, for instance for micro-total-analytical-systems[21] and lab-on-a-chip applications.[22]

In this paper, we use ac voltammetry, where the voltage is a superposition of a "slow" ramp with a large-amplitude, high-frequency harmonic oscillation, to study the electrochemical reaction-diffusion process in combination with a new signal processing method valid for analyzing the inherently nonlinear and nonstationary current response.[23,24] The aim is to develop new techniques for the fast and accurate determination/monitoring of all species- and process-specific parameters. To do so, a series of numerical simulations was conducted for different voltage excitation parameters as well as kinetic, thermodynamic and mass transport parameters. For these calculations, a number of scaling laws and similarity regions arise that are related to the underlying parameters/dynamics of the process. Under certain conditions, these observations allow the determination of all underlying parameters using standard electrode geometries and without any *a priori* assumptions regarding their value. The theoretical results derived from this analysis are compared to experiments with an outer-sphere ET species, on different electrode materials and the determined parameters are in agreement with published values.

† Present address: Division of Biology, California Institute of Technology, Pasadena, CA 91125. Tel.: +1 626 395 8965. Fax: +1 626 796 8876. E-mail: costas@caltech.edu.

10.1021/jp074585w CCC: $37.00
Published on Web 11/29/2007

2. Materials and Methods

2.1. Experimental Methods. All chemicals used in the voltammetric measurements ($Ru(NH_3)_6Cl_2$ and KCl) were purchased from Sigma-Aldrich and used as received. In all experiments the $Ru(NH_3)_6^{2+/3+}$ bulk concentration was 1 mM. KCl (1 M) was the supporting electrolyte in a two-electrode-cell (working and reference electrode). Two inlaid disc electrodes were used, one carbon fiber electrode with $r_{el}^* = 5\ \mu$m purchased from CH Instruments (Austin, Texas) and one homemade Au electrode with $r_{el}^* = 5\ \mu$m. The pretreatment of the electrodes included polishing with aqueous 1 and 0.3 μm alumina on polishing pads (Buehler) with sonication between each grade. The reference electrode was a Ag/AgCl wire in a 3 M KCl solution. Prior to experiments the solution was bubbled for 20 min with nitrogen to remove dissolved oxygen from solution. The ramped harmonic waveforms were digitally generated using Labview 7.0 software (National Instruments, Austin, Texas) and converted to an analog signal through a NI PCI 6036E card (16-bit, 200 kHz bandwidth) interfaced with an Axon Multiclamp 700B (Axon Instruments, USA).

2.2. Electrochemical Reaction-Diffusion Dynamics. We study the case where heterogeneous 1-electron electrochemical reaction between the oxidized, Ox, and the reduced form, Red, of an electrochemically active species occurs at the electrode surface according to

$$\mathrm{Ox} + \mathrm{e} \underset{k_b}{\overset{k_f}{\rightleftharpoons}} \mathrm{Red} \tag{1}$$

and diffusion is the governing mass transport process in the bulk of the solution. The equation for the nondimensional redox concentration of this case in cylindrical coordinates assuming axis-symmetry is

$$\frac{\partial u}{\partial \tau} = \frac{\partial^2 u}{\partial z^2} + \frac{\partial^2 u}{\partial r^2} + \frac{1}{r}\frac{\partial u}{\partial r} \tag{2}$$

with $u = C_{Red}/C_{Red,0}$ where C_{Red} (mol m^{-3}) is the solution concentration of Red and $C_{Red,0}$ (mol m^{-3}) the initial Red concentration. The initial and boundary conditions:

$$u(z, r, \tau = 0) = 1 \tag{3}$$

$$u(z \rightarrow \infty, r, \tau) = 1 \tag{4}$$

$$u(z, r \rightarrow \infty, \tau) = 1 \tag{5}$$

$$\left.\frac{\partial u}{\partial z}\right|_{z=0,0\le r\le r_{el}} = \exp\{(1-\alpha)\xi_n\}u - \exp\{-\alpha\xi_n\}(1-u) \tag{6}$$

$$\left.\frac{\partial u}{\partial z}\right|_{z=0,r>r_{el}} = 0 \tag{7}$$

$$\left.\frac{\partial u}{\partial r}\right|_{z,r=0} = 0 \tag{8}$$

and the faradaic current response:

$$i_{far} = \int_0^{r_{el}} \left(\left.\frac{\partial u}{\partial z}\right|_{z=0,0\le r\le r_{el}}\right) r\, dr \tag{9}$$

Equations 2−9 are expressed in dimensionless quantities and the process-characteristic properties used to nondimensionalize the system of equations are

$$\hat{t} = \frac{D}{k_0^2} \qquad \hat{z} = \frac{D}{k_0} \qquad \hat{E} = \frac{R_g T}{F} \qquad \hat{I} = 2\pi F D^2 \frac{C_{Red,0}}{k_0} \tag{10}$$

where D (m^2 s^{-1}) is the diffusion coefficient assumed to be equal for Ox and Red, k_0 (m s^{-1}) is the kinetic constant and $\alpha(-)$ the ET coefficient according to the Butler−Volmer theory,[3] F (96485.3 C mol^{-1}) is the Faraday constant, R_g (8.314 C V mol^{-1} K^{-1}) is the universal gas constant, and T (298.15 K) is the temperature. The characteristic properties in eq 10 are used to define the following dimensionless parameters:

$$\tau = \frac{t}{\hat{t}} \qquad z = \frac{z^*}{\hat{z}} \qquad r = \frac{r^*}{\hat{z}}$$

$$\xi_n = \frac{E^* - E_0^*}{\hat{E}} = \xi - \frac{E_0^*}{\hat{E}} \qquad i = \frac{I}{\hat{I}} \tag{11}$$

where τ is the dimensionless time, z and r are the coordinates in cylindrical space (z^* and r^* (m) are the dimensional forms of the cylindrical coordinates and r_{el} in eq 9 is the dimensionless electrode radius), and E_0^* (V) is the formal oxidation potential. The capacitance contribution to the overall current response i_{cap} due to the ion re-organization at the electrode surface, often referred to as double-layer capacitance for high supporting electrolyte concentrations,[3] is

$$i_{cap} = \frac{\hat{E}}{\hat{z}^3}\lambda\frac{\partial \xi}{\partial \tau}$$

with

$$\lambda = \frac{C_{dl}(r_{el}^*)^2}{2FC_{Red,0}} \tag{12}$$

where λ is the combined contribution of the double layer capacitance C_{dl} (F m^{-2}), the system-specific electrode radius r_{el}^* (m), and $C_{Red,0}$ and the species-specific $\hat{z}$ (m). As seen by eq 12, an increase in C_{dl} and r_{el}^* enhances the influence of i_{cap}, hence the benefit of using small electrodes where the capacitance contribution is decreased. Here we assume that the overall current response is a superposition of the faradaic and the capacitance components, *i.e.*, $i = i_{far} + i_{cap}$. Though strictly not true, for a small cell ohmic drop this superposition often yields a good approximation of the overall current response, particularly for outer-sphere ET as studied here, and has been widely used to simulate the capacitance interference in voltammetry.[3,23,25−27]

Note that in the theoretical model described above we have neglected uncompensated resistance R_u (Ω), *i.e.*, the solution resistance between the working electrode and the equipotential surface that transverses the tip of the reference electrode (for an insightful review of this phenomenon the interested reader is referred to refs 28 and 29). R_u, which depends on process parameters such as the solution conductivity, the location of the reference electrode probe, the counter electrode characteristics and the cell size, may influence the driving force of the heterogeneous electrochemical reaction.[3] In the present study we chose to neglect R_u because of (i) the use of micrometer-sized working electrodes and (ii) the presence of high supporting electrolyte concentrations (>0.1 M). Under such conditions, typically $R_u = 1-300\ \Omega$.[3,27] As seen in Figure 1B, from the resulting current response I, the applied voltage greatly exceeds the effect of the IR_u-drop.

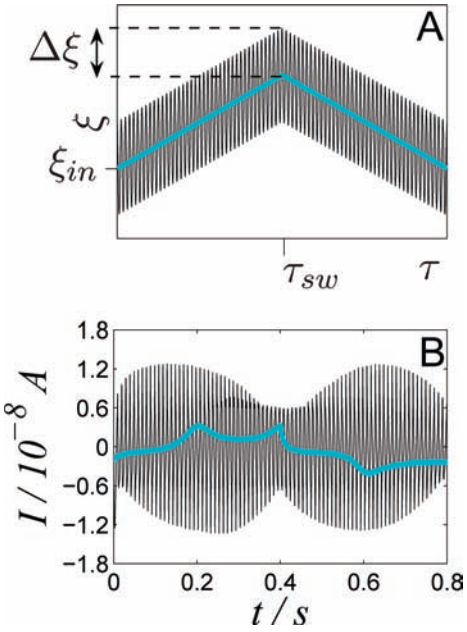

Figure 1. (A) The ac voltammetry (black) and cyclic voltammetry (cyan) excitation and (B) the current response using a 1 mM $Ru(NH_3)_6^{2+/3+}$ solution in the presence of 1 M KCl on a 5 μm Au electrode. The experimental conditions are reported in Materials and Methods.

We assume a dimensionless voltage excitation, $\xi = \xi_{dc} + \xi_{ac}$, given by

$$\xi_{dc} = \xi_{in} + \frac{\upsilon\hat{t}}{\hat{E}}\tau = \frac{E^*_{in}}{\hat{E}} + \frac{\upsilon\hat{t}}{\hat{E}}\tau \qquad \text{for } 0 \le \tau \le \tau_{sw} \tag{13}$$

$$= \xi_{in} + \frac{\upsilon\hat{t}}{\hat{E}}(2\tau_{sw} - \tau) = \frac{E^*_{in}}{\hat{E}} + \frac{\upsilon\hat{t}}{\hat{E}}(2\tau_{sw} - \tau) \qquad \text{for } \tau_{sw} < \tau \le 2\tau_{sw} \tag{14}$$

$$\xi_{ac} = \Delta\xi \cos(2\pi\hat{t}f^*\tau) = \frac{\Delta E^*}{\hat{E}} \cos(2\pi\hat{t}f^*\tau) \tag{15}$$

where E^*_{in} (V) is the initial voltage, υ (V s^{-1}) is the dc scan-rate, $\tau_{sw} = (t_{sw}/\hat{t})$ is the dimensionless dc switching time, ΔE^* (V) is the amplitude, and f^* (Hz) is the frequency of the ac excitation. In Figure 1A, the voltage excitation in CV (ξ_{dc}) is shown in cyan and the ac voltammetry excitation (ξ) is shown in black. All reaction-diffusion simulations were conducted using a commercial software package (COMSOL) on two Linux dual-processor workstations. Details regarding the performance of the numerical integrator are provided in section A in the Supporting Information.

2.3. Time-Series Analysis. The analysis applied to the numerical results defines two components of the current response i, the temporally "even" component, $g(\tau)$, and the "odd", $w(\tau)$:

$$g(\tau) = \frac{1}{2}[i(\tau) + i(2\tau_{sw} - \tau)] \tag{16}$$

$$w(\tau) = \frac{1}{2}[i(\tau) - i(2\tau_{sw} - \tau)] \tag{17}$$

The capacitance contributions, as described through eq 12, are absent from $g(\tau)$ and present only in $w(\tau)$ (for a more detailed description of this procedure see ref 24). To minimize the effect of capacitance in $w(\tau)$, the Hilbert transform (HT),

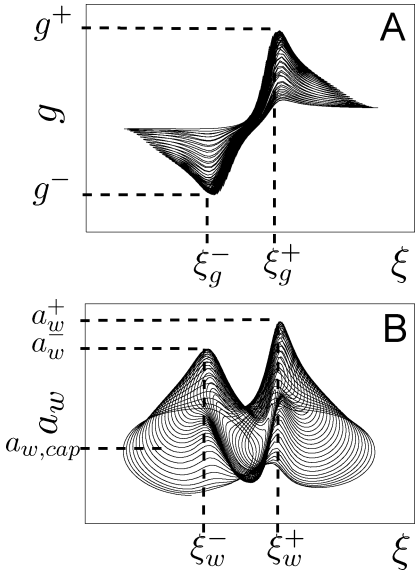

Figure 2. Characteristic envelopes resulting when eqs 16 and 17 are applied to a simulated ac voltammogram. (A) In $g(\tau)$ vs $\xi(\tau)$, capacitance contributions are absent due to the definition of i_{cap}. The characteristic envelope properties used in the analysis are (ξ_g^-, g^-) and (ξ_g^+, g^+). (B) From $a_w(\tau)$ vs $\xi(\tau)$, (ξ_w^-, a_w^-) and (ξ_w^+, a_w^+) are used for the analysis. The offset $a_{w,cap}$ is related to double-layer capacitance contributions.

as defined by Gabor,[30] is used to calculate the instantaneous amplitude $a_w(\tau)$ and the instantaneous frequency $f_w(\tau)$ of $w(\tau)$ with

$$w(\tau) + \mathrm{j}\mathcal{H}\{w(\tau)\} = a_w(\tau)\exp\{2\pi\mathrm{j}f_w(\tau)\} \tag{18}$$

where j is the imaginary number and $\mathcal{H}\{\}$ is the HT. In Figure 2, the two attributes of the current response versus the applied voltage ξ are shown: in Figure 2A, $g(\tau)$ versus $\xi(\tau)$, and in Figure 2B, $a_w(\tau)$ versus $\xi(\tau)$. The subsequent sections will focus on features of these properties of the current response to the prescribed voltage excitation ξ. More specifically, four properties are defined:

$$\Delta\xi_g = \xi_g^+ - \xi_g^- \qquad \Delta\xi_w = \xi_w^+ - \xi_w^+ \tag{19}$$

$$\gamma_g = \frac{|g^-| - |g^+|}{|g^-| + |g^+|} \qquad \gamma_w = \frac{a_w^- - a_w^+}{a_w^- + a_w^+ - 2a_{w,cap}} \tag{20}$$

where ξ_g^- and ξ_g^+ are the voltages at the two extrema in g, g^- and g^+, defined in Figure 2A, and ξ_w^- and ξ_w^+ are the voltages at the two maxima in a_w, a_w^- and a_w^+, defined in Figure 2B.

3. Results and Discussion

A series of numerical simulations was conducted to explore the changes of $\Delta\xi_g$, $\Delta\xi_w$, γ_g, and γ_w for different sets of species- and process-specific parameters. The following species-specific parameter space was explored in the numerical simulations: $10^{-5} \le (k_0/\mathrm{m\ s^{-1}}) \le 10^{-2}$, $10^{-10} \le (D/\mathrm{m^2\ s^{-1}}) \le 10^{-9}$, $0.3 \le \alpha \le 0.7$. For the present analysis, $r^*_{el} = 3.5 \times 10^{-6}$ m and $C_{dl} = 10^{-1}$ C V^{-1} m^{-2}. These values are typical for medium to fast heterogeneous electrochemical reaction kinetics in aqueous solution measured using conventional disc microelectrodes.

To investigate the effect of the voltage input, different sets of parameters of the ac voltammetry excitation, *i.e.*, the voltage parameter space, were studied. The excitations shown are (1)

$\upsilon = 0.2$ V s^{-1}, $f^* = 10$ Hz, (2) $\upsilon = 1$ V s^{-1}, $f^* = 50$ Hz, (3) $\upsilon = 2$ V s^{-1}, $f^* = 100$ Hz, and (4) $\upsilon = 10$ V s^{-1}, $f^* = 500$ Hz. In all cases, the harmonic excitation amplitude $\Delta E^* = 0.4$ V and the characteristic excitation number $(\Delta E^* f^*/\upsilon) = 20$ because this particular value has been shown to offer enhanced voltammetric detail.[31]

For all simulations, E_0^* was accurately determined from the voltage midway between the extrema in both attributes of the current response:

$$\frac{E_0^*}{\hat{E}} = \frac{\xi_g^- + \xi_g^+}{2} \quad \text{and} \quad \frac{E_0^*}{\hat{E}} = \frac{\xi_w^- + \xi_w^+}{2} \tag{21}$$

Because for all voltage excitation investigated $f^* \gg \upsilon/\Delta E^*$, given that the capacitance contribution is only present in the odd component and from the definition of the instantaneous amplitude a_w it can be shown that

$$\lambda = \frac{\hat{z}^3}{\hat{E}\,\Omega\,\Delta\xi} a_{w,\mathrm{cap}} \tag{22}$$

where $\Omega = 2\pi f^* \hat{t}$ is the dimensionless angular excitation frequency.

The results of the numerical simulations are illustrated in Figure 3 where the voltage separation of the even $\Delta\xi_g$ and the instantaneous amplitude of the odd component $\Delta\xi_w$ of the signal are plotted versus two dimensionless groups. It was found empirically that these dimensionless groups collapse the simulation results for $\alpha = 0.5$ for all of the voltage excitations. In Figure 3, the circles indicate the position where $\alpha = 0.5$ whereas the bars are the range due to $0.3 \le \alpha \le 0.7$. The voltage excitations, according to the definition given above, are (1) black, (2) blue, (3) cyan, and (4) magenta.

In Figure 3A, $\Delta\xi_w$ is shown as a function of the dimensionless group $(D f^*/k_0^2)$ and it is observed that all results align very well with this simple scaling. Moreover, it is observed that sluggish kinetics (small k_0) result in larger $\Delta\xi_w$ as already known from CV.[8] For all curves, $(Df^*/k_0^2) = 10^{-1}$ represents a limit below which $\Delta\xi_w = 0$. The fact that $\Delta\xi_w$ scales with (Df^*/k_0^2) for such a wide voltage and species parameter space indicates the presence of a dominant effect/process described by the latter parameter.

In Figure 3B, $\Delta\xi_g$ is shown versus the dimensionless group $(D\Delta E^*/r_{\mathrm{el}}^{*2}\upsilon)(r_{\mathrm{el}}^* f^*/k_0)^\beta$, which is a function of species- and process-specific parameters as well as the parameter β. β is a parameter that aligns all cases when $\alpha = 0.5$ and depends on the applied excitation as seen on Figure 3C, where β is shown versus the applied excitation frequency f^* for $\Delta E^* = 0.4$ V and $(\Delta E^* f^*/\upsilon) = 20$. As in Figure 3A, sluggish kinetics result in larger $\Delta\xi_g$ with the exact functionality of this behavior depending on the parameters of the dimensionless group $(D\Delta E^*/r_{\mathrm{el}}^{*2}\upsilon)(r_{\mathrm{el}}^* f^*/k_0)^\beta$, which is a combination of the 'slow' term $(D\Delta E^*/r_{\mathrm{el}}^{*2}\upsilon)$ and the "fast" term $(r_{\mathrm{el}}^* f^*/k_0)^\beta$.[38] For slower excitations, $f^* \le 50$ Hz, there is a linear relation between β and f^*. For $f^* \ge 100$ Hz, $\beta = 1.7$. As a result, the behavior shown in Figure 3B for the voltage excitation (4) where $f^* = 500$ Hz (magenta) is representative of all excitations for $f^* \ge 250$ Hz. It is interesting to note that for slow excitations $\Delta\xi_g$ scales with $(D/k_0 r_{\mathrm{el}}^*)$ whereas for fast excitations (Df^*/k_0^2). This effect is attributed to the spatiotemporal concentration profiles close to the electrode surface, as indicated in the analysis shown in section C in the Supporting Information.

From these results we can see that this signal processing method offers new insights into voltammetric reaction-diffusion dynamics. For slower excitations, the voltage-spacing between the extrema in the two attributes of the current response, g and a_w, scale according to different dimensionless groups. For fast excitations, both attributes of the current response are dominated by $(D f^*/k_0^2)$. This behavior can potentially be related to the spatiotemporal patterns shown in the Supporting Information where it is observed that, while a homogeneous concentration gradient is observed for slow excitations, the spatial concentration inhomogeneities become significant for fast excitations.

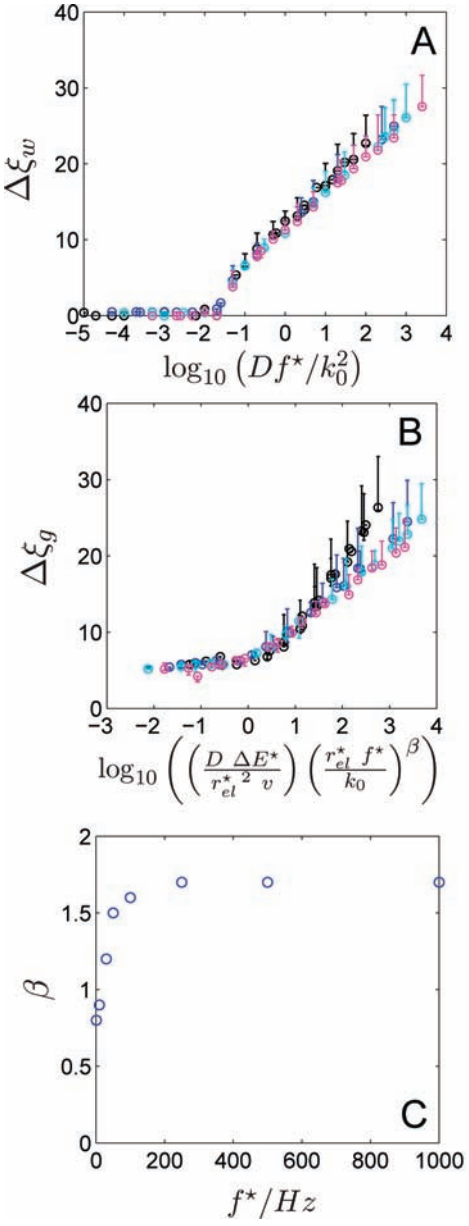

Figure 3. Analysis of the odd (A) and the even (B and C) component of a series of numerical simulations. The different colors in (A) and (B) indicate the voltage excitation: $\upsilon = 0.2$ V s^{-1}, $f^* = 10$ Hz (black); $\upsilon = 1$ V s^{-1}, $f^* = 50$ Hz (blue); $\upsilon = 2$ V s^{-1}, $f^* = 100$ Hz (cyan); $\upsilon = 10$ V s^{-1}, $f^* = 500$ Hz (magenta). The circles indicate simulation results for $\alpha = 0.5$, and the bars, the range due to $0.3 \le \alpha \le 0.7$.

The following regressions are derived from the scaling illustrated in Figure 3A,B:

$$\Delta\xi_g = a_1 \ln\left\{\frac{D\Delta E^*}{r_{\mathrm{el}}^{*2}\upsilon}\left(\frac{r_{\mathrm{el}}^* f^*}{k_0}\right)^\beta\right\} + b_1 \tag{23}$$

$$\Delta\xi_w = a_2 \ln\left\{\frac{Df^*}{k_0^{\ 2}}\right\} + b_2 \tag{24}$$

TABLE 1: Interpolation Parameters for Different Voltage Excitations

υ/V s^{-1}	f^*/Hz	a_1	b_1	a_2	b_2
0.02	1	3.71	2.05	2.39	11.81
0.2	10	4.25	−0.39	2.39	11.81
0.6	30	3.04	3.68	2.19	11.33
1	50	2.39	5.37	2.15	11.38
2	100	2.17	5.79	2.18	11.01
5	250	2.00	6.08	2.07	11.33
10	500	1.95	6.16	2.09	11.03
20	1000	1.89	6.33	2.10	10.83

where a_1, a_2, b_1, and b_2 are parameters of the regressions and β is the aligning parameter introduced for $\Delta\xi_g$ shown in Figure 3C. It has to be mentioned that these regressions are for $(D\Delta E^*/r_{el}^{*2}\upsilon)(r_{el}^* f^*/k_0)^\beta > 1$ and $(Df^*/k_0^2) > 10^{-2}$. Table 1 illustrates the values of the regression-parameters for the different voltage excitations and the trends mentioned earlier can be clearly observed: for $f^* > 100$ Hz, all excitations result in the same $\Delta\xi_g$-scaling ($a_1 \approx 2$ and $b_1 \approx 6$) whereas the $\Delta\xi_w$-scaling depends only on the characteristic excitation number ($\Delta E^* f^*/\upsilon$) ($a_2 \approx 2.1$ and $b_2 \approx 11$). From eqs 23 and 24 it is possible to determine the kinetic constant k_0 through

$$k_0 = \left(\frac{(r_{el}^*)^{2-\beta}(f^*)^{1-\beta}\upsilon}{\Delta E^*}\right)^{1/(2-\beta)} \exp\left\{\frac{1}{2-\beta}\left(\frac{\Delta\xi_g - b_1}{a_1} - \frac{\Delta\xi_w - b_2}{a_2}\right)\right\} \quad (25)$$

The extent to which eq 25 adequately predicts the k_0 depends on the excitation characteristics as well as the particular species investigated. Nevertheless, it is observed that for $f^* \simeq 20$ Hz where, according to Figure 3B, $\beta = 1$, eq 25 becomes

$$k_0 = \left(\frac{r_{el}^*\upsilon}{\Delta E^*}\right)\exp\left\{\frac{\Delta\xi_g - b_1}{a_1} - \frac{\Delta\xi_w - b_2}{a_2}\right\} \quad (26)$$

In general, the fact that faster excitations have a larger β-value can lead to errors in the determination of k_0 because of the presence of β in the exponential function in eq 25. As a result, measurements with species where $\alpha \neq 0.5$ are predicted to have a larger effect on fast excitations. The same applies for experimental inaccuracies, which can lead to erroneous predictions, especially for fast excitations. Another important feature arising from eqs 25 and 26 is that, while small electrode sizes favor the measurement of large k_0 (Figure 3A), this also depends on the voltage excitation; while for slow excitations $r_{el}^* = \mathcal{O}(1)$, for fast excitations $r_{el}^* = \mathcal{O}(0.3)$ and thus the electrode size-effect is damped.

The formulation used to determine the diffusion coefficient D is also derived from eqs 23 and 24:

$$D = \left[\frac{\Delta E^*}{r_{el}^{*2}\upsilon}\left(\frac{r_{el}^* f^*}{k_0}\right)^\beta\right]^{-a_1/(a_1+a_2)}\left[\frac{f^*}{k_0^2}\right]^{-a_2/(a_1+a_2)} \exp\left\{\frac{\Delta\xi_g + \Delta\xi_w - (b_1+b_2)}{a_1+a_2}\right\} \quad (27)$$

In this expression, D exhibits the same voltage excitation-dependent functionality on r_{el}^* as k_0. However, D is only implicitly dependent on parameter β through k_0. Because the order of the dependence of D on k_0 is always greater than 1 (see eq 27 and Table 1), inaccuracies in the determination of k_0 result in large errors in the value of D. Hence, the considerations regarding the accurate determination of k_0 also apply for the determination of D.

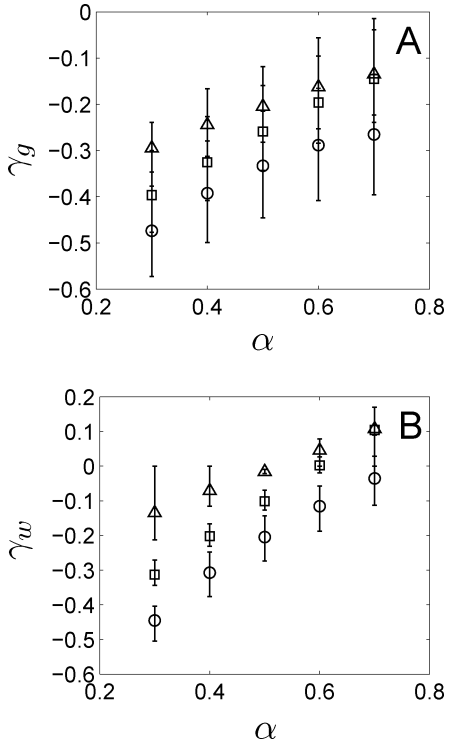

Figure 4. Effect of α on the extema symmetry factors γ_g (A) and γ_w (B). Results for $D = 5 \times 10^{-10}$ m^2 s^{-1} and three variations of k_0 are shown: $k_0 = 10^{-5}$ m s^{-1} (○); 10^{-4} m s^{-1} (□); 10^{-3} m s^{-1} (△). The symbols represent the mean for the voltage excitations (2)−(4) where (2) $\upsilon = 1$ V s^{-1} and $f^* = 50$ Hz, (3) $\upsilon = 2$ V s^{-1} and $f^* = 100$ Hz, and (4) $\upsilon = 10$ V s^{-1} and $f^* = 500$ Hz. The bars represent the range. For all cases, there is a linear relationship between both symmetry factors and α with the variations due to the different excitation being less pronounced in γ_w vs α.

For electrochemical systems with $D/k_0^2 < 10^{-3}$ s, such as $IrCl_6^{4-/3-}$,[33] where the determination of the individual parameters becomes problematic, determining the species-specific characteristic time D/k_0^2 can provide an attractive alternative to the individual determination of D and k_0 for two reasons: (i) because $\beta \approx \mathcal{O}(2)$, both attributes of the current response, g and a_w, provide information about this ratio, which enhances the level of confidence, and (ii) because the diffusion coefficient D in aqueous solutions normally varies within 1 order of magnitude ($D = 10^{-10}$−10^{-9} m^2 s^{-1}), k_0 can be determined from this ratio alone within approximately 50% accuracy.

The symmetry parameters γ_g and γ_w defined through eq 20 are used to determine the ET coefficient α as a function of the symmetry of the extrema.[24] In Figure 4, γ_g (A) and γ_w (B) are shown as a function of α for a number of simulations where $D = 5 \times 10^{-10}$ m^2 s^{-1} and three values of k_0: 10^{-5} m s^{-1} (○), 10^{-4} m s^{-1} (□) and 10^{-3} m s^{-1} (△). The results for the voltage excitations (2)−(4) are illustrated, and the symbols represent the means for the three values of k_0 and the bars the range due to the different voltage excitations. As observed, for all cases, there is a linear relation between both symmetry factors and α. Moreover, it is shown that the variations due to the different excitation are less pronounced in γ_w versus α than in γ_g versus α where there is significant overlap in the range. This is due to the fact that the reference in g versus ξ is also a function of the mobility of the species.[24] Therefore, determination of α from the a_w versus α representation offers enhanced accuracy compared to g versus α.

TABLE 2: Experimental Results Based on Figure 5

	$Ru(NH_3)_6^{2+/3+}$ on Au		$Ru(NH_3)_6^{2+/3+}$ on carbon fiber	
	Figure 5	refs 3 and 35	Figure 5	refs 33, 35, and 37
k_0/m s^{-1}	9×10^{-4}	2.9×10^{-3}	6×10^{-4}	2×10^{-3}
D/m^2 s^{-1}	4×10^{-10}	$(5-7) \times 10^{-10}$	4×10^{-10}	$(5-7) \times 10^{-10}$
α	0.6	(0.5)	0.5	(0.5)
E_0^*/mV vs Ag/AgCl	−190	−218	−190	−185
C_{dl}/F m^2	0.2	0.01−0.3	0.1	0.1−0.7

Based on the theoretical analysis presented here, $Ru(NH_3)_6^{2+/3+}$ which has been shown to undergo outer-sphere ET, was studied using ac voltammetry and two disk microelectrodes with different materials, Au and carbon fiber. The CV response for both experiments is shown in g versus ξ (cyan) with υ being the same as for each ac voltammetry excitation. Two voltage excitations were used; for the Au electrode $\upsilon = 2$ V s^{-1} and $f^* = 100$ Hz (the overall current response is shown in Figure 1B) while for the carbon fiber electrode $\upsilon = 1$ V s^{-1} and $f^* = 50$ Hz. To analyze the experimental data, the following steps were carried out:

(1) Decompose the current response into the components $g(t)$ and $w(t)$ according to eq 16 and 17.

(2) From the representation g versus ξ, define $\Delta\xi_g$, eq 19, and the ratio γ_g, eq 20.

(3) Calculate the instantaneous amplitude a_w of the analytic signal of w,[30,34] to suppress the influence of capacitance and from the representation a_w versus ξ define the voltage $\Delta\xi_w$, eq 19, and the ratio γ_w, eq 20.

(4) From the midway-voltage in g versus ξ and a_w versus ξ, determine E_0^* using eq 21.

(5) From the two characteristic values, $\Delta\xi_g$ and $\Delta\xi_w$, deduce k_0 and D separately from eqs 25 and 27 (or, if impossible, D/k_0^2 from the same equations).

(6) From the characteristic ratios γ_g and γ_w, determine α from Figure 4.

(7) From the offset of the instantaneous amplitude $a_{w,cap}$ and eq 22, determine the double-layer capacitance C_{dl}.

The results of this analysis are shown in Table 2 and are based on the even and odd attribute of the current response shown in Figure 5, which is representative of three consecutive experiments with the same electrode. It is observed that the values determined are in good agreement with those given by Khoshtariya and co-workers,[35] who measured k_0 on bare gold electrodes using CV and Nicholson's analysis with the same supporting electrolyte.[8] The same applies for the measurements using carbon fiber electrodes. The species-specific parameters are in good agreement with the ones measured by Chen et al.[33] who used glassy carbon electrodes and the software package Digisim[36] to determine k_0 by fitting the peak-to-peak distance for a given υ and assuming $\alpha = 0.5$ *a priori*. Nevertheless, it has to be noted that because for $Ru(NH_3)_6^{2+/3+}$ the characteristic time $\hat{t} = 10^{-4}-10^{-3}$ s, it is in the region where the accurate determination of the species parameters becomes difficult according to the analysis shown in Figure 3.

The double-layer capacitance C_{dl}, estimated through eq 22, is in good agreement with literature values, although the assumption that the overall capacitance contribution is present only in $w(t)$ is shown not to be true. Nevertheless, as seen in Figure 5D, even an irregular capacitance contribution is minimized very efficiently using the HT. As observed there, the capacitance current contribution changes by approximately 50%, from $a_{w,cap} = 12 \times 10^{-10}$ A to 6×10^{-10} A during the experiment.

4. Conclusions

In this paper, new tools for the time-series analysis of voltammetric experiments are applied to numerical ac voltammetric reaction-diffusion data simulating the spatiotemporal dynamics at microelectrodes. Sensitivity analyses are conducted both on the voltage excitation space (2 orders of magnitude in the excitation-characteristic time $1/f^*$) and in the species parameter space ($10^{-10} \leq (D/\text{m}^2\ \text{s}^{-1}) \leq 10^{-9}$ and $0.3 \leq \alpha \leq$

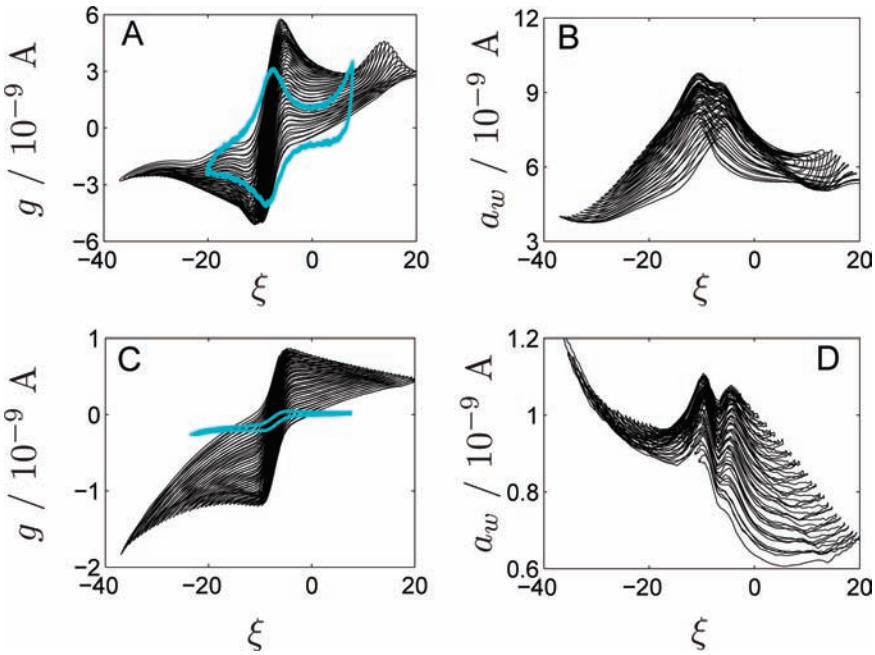

Figure 5. Experiments with 1 mM $Ru(NH_3)_6^{2+/3+}$ in 1 M KCl on a $r_{el}^* = 5$ μm Au electrode, (A) and (B), and on a $r_{el}^* = 5$ μm carbon fiber electrode, (C) and (D). In (A) and (C) component g is shown whereas in (B) and (D) a_w is given. For the Au electrode the voltage excitation used was $\upsilon = 2$ V s^{-1}, $f^* = 100$ Hz whereas for the carbon fiber electrode $\upsilon = 1$ V s^{-1}, $f^* = 50$ Hz. In both experiments $\Delta E^* = 0.4$ V. In (A) and (C), the CV response for both systems is shown (cyan) for the same υ as for the ac voltammetry experiments.

0.7). These values are commonly encountered in voltammetric experiments. The analysis offered new insights into the functionality and scaling of these processes: while $\Delta\xi_w$-scaling proved robust for all voltage excitations, $\Delta\xi_g$-scaling depends on the applied voltage. These scaling-laws enabled the fast and accurate determination of all species-specific parameters, the heterogeneous kinetic reaction constant k_0, the diffusivity D, the ET coefficient α, and the formal oxidation potential E_0^* as well as the capacitance C_{dl}, without any *a priori* assumptions or any specialized electrode geometry. Despite the use of a simple model, *i.e.*, Butler−Volmer kinetics in parallel with a linear capacitor, experiments using Au and carbon fiber microelectrodes and an outer-sphere electrochemical couple exhibited the accuracy this methodology offers. Moreover, the short duration of each experiment, for voltage excitation (1) $2t_{sw} = 8$ s, for (2) $2t_{sw} = 1.6$ s, for (3) $2t_{sw} = 0.8$ s, and for (4) $2t_{sw} = 0.16$ s, and the fast time-series analysis (for conventional processors in the order of 1 s) leads to the very rapid determination of the species-specific parameters that is important for a number of chemical, biological, and environmental monitoring applications.

Nomenclature

Latin Symbols

a_1, a_2 : regression slope parameters (−)

a_w : instantaneous amplitude of $w(\tau)$ (-)

b_1, b_2 : regression offset parameters (-)

c_{Red} ($C_{Red,0}$) : solution concentration of the reduced species (initially) (mol m^{-3})

C_{dl} : double layer capacitance (F m^{-2})

D : diffusion coefficient (m^2 s^{-1})

e : electron charge (1.6022×10^{-19} C)

E^*, E_0^* : imposed voltage and formal oxidation potential (V)

f^*, f_w : ac voltage excitation frequency (s^{-1}) and instantaneous frequency (s^{-1})

g : temporally "even" component (−)

$\mathcal{H}\{\}$: Hilbert transform

I, i : current (A) and dimensionless current (−)

j : imaginary number

k_0, k_f, k_b : kinetic constant (Butler−Volmer theory) and of the forward and backward reaction (s^{-1})

$\mathcal{O}$: order

Ox : oxidized species

r, r_{el} : radial coordinate and electrode radius (m)

Red : reduced species

u : dimensionless solution concentration of Red (−)

v : voltage dc scan rate (V s^{-1})

w : temporally odd component (−)

z : vertical coordinate

Greek Symbols

α : charge-transfer coefficient (−)

β : alignment parameter (−)

γ : envelope maxima ratio (−)

ΔE^* : voltage excitation amplitude (V)

$\Delta\xi$: dimensionless voltage difference (−)

λ : dimensionless double layer/electrode radius contribution (−)

ξ, ξ_n : dimensionless voltage and normalized voltage (−)

τ, τ_{sw} : dimensionless time and dc switching time (−)

Ω : dimensionless angular excitation frequency (−)

Accents and Superscripts

$\wedge$: characteristic properties

* : dimensional system- and voltage-excitation parameters

− : extremum for $\xi_n < 0$

+ : extremum for $\xi_n > 0$

Subscripts

cap : capacitance component

far : Faradaic component

Physical Constants

F : Faraday constant (C mol^{-1})

R_g : universal gas constant (C V mol^{-1} K^{-1})

T : temperature (K)

Acknowledgment. This article is dedicated to the memory of Prof. Dr. M. John Lever for supporting this research. C.A.A. thanks the EPSRC for the financial support as well as Dr. M. Barahona and Dr. A. A. Bharath for CPU time.

Supporting Information Available: In section A, details regarding the method and the performance of the numerical integration are provided. In section B, the MATLAB algorithm for the numerical calculation of the instantaneous amplitude is given, and in section C, spatiotemporal concentration profiles numerically calculated for two sinusoidal voltammetry excitations are shown. The material is available free of charge via the Internet at http://pubs.acs.org.

References and Notes

(1) Wightman, R. M. *Science* **2006**, *311*, 1570−1574.
(2) Heinze, J. *Angew. Chem., Intern. Ed.* **1993**, *32*, 1268−1288.
(3) Bard, A. J.; Faulkner, L. R. *Electrochemical methods*; Wiley & Sons: New York, 2001.
(4) Armstrong, F. A. *Chem. Soc. Rev.* **1997**, *26*, 169−179.
(5) Wang, G. L.; Bohaty, A. K.; Zharov, I.; White, H. S. *J. Am. Chem. Soc.* **2006**, 128, 13553−13558.
(6) Heien, M. L. A. V.; Khan, A. S.; Ariansen, J. L.; Cheer, J. F.; Phillips, P. E. M.; Wassum, K. M.; Wightman, R. M. *Proc. Natl. Acad. Sci. U.S.A.* **2005**, *102*, 10023−10028.
(7) Zhou, F. M.; Liang, Y.; Salas, R.; Zhang, L.; De Biasi, M.; Dani, J. A. *Neuron* **2005**, *46*, 65−74.
(8) Nicholson, R. S. *Anal. Chem.* **1965**, *37*, 1351−1355.
(9) Nicholson, R. S.; Shain, I. *Anal. Chem.* **1964**, *36*, 706−723.
(10) Rees, N. V.; Alden, J. A.; Dryfe, R. A. W.; Coles, B. A.; Compton, R. G. *J. Phys. Chem.* **1995**, *99*, 14813−14818.
(11) Macpherson, J. V.; Jones, C. E.; Unwin, P. R. *J. Phys. Chem. B* **1998**, *102*, 9891−9897.
(12) Melville, J. L.; Simjee, N.; Unwin, P. R.; Coles, B. A.; Compton, R. G. *J. Phys. Chem. B* **2002**, *106*, 2690−2698.
(13) Melville, J. L.; Coles, B. A.; Compton, R. G.; Simjee, N.; Macpherson, J. V.; Unwin, P. R. *J. Phys. Chem. B* **2003**, *107*, 379−386.
(14) Macpherson, J. V.; Simjee, N.; Unwin, P. R. *Electrochim. Acta* **2001**, *47*, 29−45.
(15) Bitziou, E.; Rudd, N. C.; Edwards, M. A.; Unwin, P. R. *Anal. Chem.* **2006**, *78*, 1435−1443.
(16) Penner, R. M.; Heben, M. J.; Longin, T. L.; Lewis, N. S. *Science* **1990**, *250*, 1118−1121.
(17) White, R. J.; White, H. S. *Anal. Chem.* **2005**, 77, 214A− 220A.
(18) Wipf, D. O.; Bard, A. J. *J. Electroanal. Chem.* **1991**, *138*, 469−474.
(19) Bard, A. J.; Mirkin, M. V.; Unwin, P. R.; Wipf, D. O. *J. Phys. Chem.* **1992**, *96*, 1861−1868.
(20) Wittstock, G.; Burchardt, M.; Pust, S. E.; Shen, Y.; Zhao, C. *Angew. Chem., Int. Ed.* **2007**, *46*, 1584−1617.
(21) Wang, J.; Polsky, R.; Tian, B. M.; Chatrathi, M. P. *Anal. Chem.* **2000**, *72*, 5285−5289.
(22) Whitesides, G. M. *Nature* **2006**, *442*, 368−373.
(23) Bond, A. M.; Duffy, N. W.; Guo, S. X.; Zhang, J.; Elton, D. *Anal. Chem.* **2005**, *77*, 186A-196A.
(24) Anastassiou, C. A.; Ducros, N;, Parker, K. H.; O'Hare, D. *Anal. Chem.* **2006**, *78*, 4383−4389.
(25) Engblom, S. O.; Myland, J. C.; Oldham, K. B. *J. Electroanal. Chem.* **2000**, *480*, 120−132.
(26) Gavaghan, D. J.; Bond, A. M. *J. Electroanal. Chem.* **2000**, *480*, 133−149.
(27) Sher, A. A.; Bond, A. M.; Gavaghan, D. J.; Harriman, K.; Feldberg, S. W.; Duffy, N. W.; Guo, S. X.; Zhang, J. *Anal. Chem.* **2004**, *76*, 6214−6228.

(28) Myland, J. C.; Oldham, K. B. *Anal. Chem.* **2000**, *72*, 3972−3981.
(29) Oldham, K. B.; Stevens, N. P. C. *Anal. Chem.* **2000**, *72*, 3981−3988.
(30) Gabor, D. *Proc. IEE* **1946**, *93*, 429−457.
(31) Anastassiou, C. A.; Patel, B. A.; Arundell, M.; Yeoman, M. S.; Parker, K. H.; O'Hare, D. *Anal. Chem.* **2006**, *78*, 6990−6998.
(32) Aoki, K.; Akimoto, K.; Tokuda, K.; Matsuda, H.; Osteryoung, J. *J. Electroanal. Chem.* **1984**, *171*, 219−230.
(33) Chen, P.; Fryling, M. A.; McCreery, R. L. *Anal. Chem.* **1995**, *67*, 3115−3122.
(34) Bendat, J. S.; Piersol, A. G. *Random data*; Wiley-Interscience: New York 2000.
(35) Khoshtariya, D. E.; Dolidze, T. D.; Ventova, A.; Longhi, M.; Rondinini, S. *Electrochem. Commun.* **2003**, *5*, 241−245.
(36) Rudolph, M.; Reddy, D. P.; Feldberg, S. W. *Anal. Chem.* **1994**, *66*, A589−A590.
(37) Kinoshita, K. *Carbon: Electrochemical-physicochemical properties*; Wiley: New York, 1988.

(38) Note that the dimensionless group $(D\Delta E^*/r_{el}^{*2}v)(r_{el}^*f^*/k_0)^\beta$ can also be written as $(R_gTD/Fvr_{el}^{*2})(F\Delta E^*/R_gT)(r_{el}^*f^*/k_0)^\beta$. In the latter group, the first term, (R_gTD/Fvr_{el}^{*2}), was introduced by Aoki et al.[32] to study linear sweep voltammetry at small disc electrodes and, since then, has often been used to study various linear sweep voltammetry and CV cases. Because in the present work the group $(F\Delta E^*/R_gT)$ is constant for all simulations, the results presented in this analysis can be readily interpreted with respect to $(R_gTD/Fvr_{el}^{*2})(r_{el}^*f^*/k_0)^\beta$. Nevertheless, the dimensionless group $(D\Delta E^*/r_{el}^{*2}v)(r_{el}^*f^*/k_0)^\beta$ used in the present work reflects the fact that the voltage excitation studied herein is a superposition of a "slow" ramp with a "fast" large-amplitude/high-frequency harmonic oscillation.